09

Aspects of image formation in compound refractive lenses in the soft X-ray wavelength range

© P.Yu. Glagolev, G.D. Demin, V.I. Korneev, N.A. Djuzhev

National Research University of Electronic Technology (MIET)
124498 Zelenograd, Moscow, Russia
e-mail: glagolev@ckp-miet.ru

Received May 17, 2024
Revised May 17, 2024
Accepted May 17, 2024

The possibility of using compound refractive lenses as elements of X-ray optics designed to form an image on an X-ray resist in the soft X-ray wavelength range is discussed. For this purpose, a mathematical simulation of the transformation of the wave front as it passes through the optical system under consideration was carried out. The intensity distribution of the X-ray radiation wavefront with a wavelength varied from 2 to 14 nm at the input/output of a compound refractive lens and in the plane of the substrate with X-ray resist is calculated. Promising materials (Si, Be, diamond) of compound refractive lenses, which have high transparency for the selected wavelengths, are considered. It has been shown that the transition to diffractive and kinoform lenses minimizes the degree of absorption of X-ray radiation in the lens material by several orders of magnitude, which makes it possible to increase the resolution up to 14 nm. The results of the study can be used in the development of new optical systems based on a transparent mask and a compound refractive lens, which are applicable for X-ray nanolithography tasks.

Keywords: X-ray nanolithography, X-ray radiation, compound refractive lens, kinoform lenses, resolution, numerical aperture.

DOI: 10.61011/TP.2024.07.58816.177-24

Introduction

In current sanction restriction and import substitution conditions, a demand for domestic nanoelectronic fabrication for the technology nodes of 28 nm and below is much more acute. To produce integrated circuits (IC) in accordance with the technology nodes mentioned above, microelectronic manufacturers shall be provided with proper technological infrastructure that will ensure fulfilment of the basic process operations, including machining and chemical processing of semiconductor wafers, mask set production, photolithography and X-ray lithography procedures, impurity doping and ohmic contact fabrication operations, wafer surface passivation, wafer slicing, chip assembling and packaging, and final batch control and marking.

Lithography is one of the key operations listed above, because it determines a technology node, productivity of the process line and final product cost. There are currently more than 20 microelectronic manufacturers in the Russian Federation that are focused on small- and medium-batch production of ICs and on the development of pilot batches in accordance with the technology nodes from several microns to 130 and 90 nm [1,2]. However, the development of 90- and 65-nm technology processes is currently underway, whereas the transition to smaller technology nodes requires a lithography system that allows achieving such a resolution. Since it is prohibited to purchase such high-tech components from foreign manufacturers, development of a domestic lithography system that provides scaling to a level of 28 nm and below is a strategic task for the country.

Until recently, the most advanced type of lithography was projection photolithography at the wavelength $\lambda = 193$ nm that used a double or triple patterning (multiple patterning) method to achieve 0.14λ (28 nm) and 0.1λ (20 nm) resolution, respectively [3]. Whereas due to multiple patterning, the number of process operations with masks increased several times and, therefore, made IC production more expensive and reduced the lithography system capacity. Modern global nanoelectronics production has already achieved the 3 nm technology node, while the 2 nm process is currently in its implementation phase. Such progress has been made due to exposure wavelength reduction towards extreme ultraviolet (EUV). For example, latest-generation EUV tools operating at $\lambda = 13.5$ nm (ASML's Twinscan NXE:3600D and NXE:3800E) have a resolution about 13 nm (half-pitch) to provide the transition to the 5 nm technology node and below [4].

Absence of a powerful EUV or X-ray source that is necessary to ensure the required microelectronic production rate (more than 100 wafers per hour) is one of the key problems in creating a domestic nanolithography system. For this, foreign EUV tools use a Sn-based laser plasma source (LPS) generating $\lambda = 13.5$ nm radiation. Some studies also address the use of Xe-based LPS with a wavelength of $\lambda = 10.8-11.2$ nm [5,6]. A LPS problem is the large vapor and plasma ion fluxes to the collector and lithography system that reduce the lithography process purity. A synchrotron source (SS) that produces powerful X-ray radiation in a wide wavelength range ($\lambda = 0.01-15$ nm) may be used as an alternative method.

In addition to the source of exposure radiation, an integral part of the nanolithography system is its optical system which focuses this radiation after it passes through the mask and defines the resolution of the image to be generated. Currently, a good development level has been achieved for multilayer X-ray mirrors (MXM) based on various types of structures — Si/Mo, Mo/Be, Ru/Be, Ru/Cr, La/B, etc. [7–10]. Such mirrors have an alternating layer structure where radiation is partially reflected from each layer and amplified due to the interference effect. However, the MXM has the following disadvantages:

1) even when record-breaking experimental reflectances in the range of 60−70% have been achieved (for Si/Mo-based mirrors with Be buffer layer — about 71% for $\lambda = 13.5$ nm, for Mo/Be-based mirrors — about 70.3% for $\lambda = 11.2$ nm [11,12] for La/B-based mirrors — about 64.1% for $\lambda = 6.6$ nm [13]), the expected energy loss in the lithography optical system consisting of 11 MXMs is in total equal to about 98−99% (radiation energy is almost completely spent to multiple reflection);

2) an overall interlayer roughness of 0.3 nm does not allow the MXM reflectance to be further increased beyond 30% at $\lambda < 6$ nm, which makes them not applicable for lithography within the specified spectral range [14,15].

To overcome the restrictions mentioned above, it is proposed to use refractive X-ray optics that has been successfully used previously in [16–18] to focus hard X-ray radiation ($\lambda < 1$ nm). Selection of such operating wavelength band is associated with the fact that soft X-ray and EUV radiation was highly absorbed by the refractive lens material and, therefore, this concept could not be developed for the case of λ variation from 1 to 10 nm and above. Disadvantages of the refractive optics may also include low refraction index resulting in large focal distance of the lens and, thus, to low numerical aperture that in turn does not allow a sufficient amount of diffracted radiation to be collected from the mask (wave front data) to obtain a sharp image.

Overcoming the above limitations will allow a considerable progress to be made in using the refractive X-ray optics for X-ray lithography, in particular, for producing experimental IC batches or X-ray masks. In addition, X-ray microscopy is a promising application of the refractive X-ray optics in the soft X-ray wavelength range. Once these constraints have been surmounted, the optical system of refractive X-ray lenses will have the following benefits:

1) the use of shorter wavelengths ($\lambda < 6.5$ nm) compared with the MXM optical system to achieve better resolution;

2) the ability to study biological objects in a „water window“ spectral range ($2.3 < \lambda < 4.4$ nm) with a resolution of 20 nm and below.

The study is focused on finding the ways to attenuate the X-ray absorption coefficient by the refractive X-ray optics in order to use the reflective X-ray optics at soft X-ray wavelengths ($\lambda = 2-14$ nm) applicable to the X-ray nanolithography tasks. To focus soft X-rays, biconcave refractive lenses should be used, in which the real part of the refractive index is less than unity. The numerical aperture may be increased by using a composite refractive lens (CRL) consisting of a set of consecutive elementary biconcave lenses [19–21]. When using N elementary biconcave lenses, the focal distance becomes N times shorter. Two key factors have a negative impact on the image formation and resolution of refractive optics: first, diffraction-induced blurring associated with the finite size of the entrance diaphragm and, second, blurring induced by radiation absorption in the lens material. In most cases, the absorption-induced factor has higher effect on formation of the final X-ray resist image. We have considered the methods for increasing the CRL resolution that reduce this factor, in particular using materials (Be, diamond) with low absorption coefficient in the soft X-ray wavelength range.

1. Theory of X-ray radiation focusing by composite refractive optics

Figure 1 shows image generation by the refractive X-ray optics for the synchrotron source (SS) case. A flat front from SS illuminates the transparent mask. The lens behind the the X-ray mask focuses the X-ray radiation onto a photoresist-coated wafer. The transparent mask is a two-layer perforated membrane with square holes. The first transparent layer serves as a carrying structure and heat sink for the radiation energy absorbed in the mask. The second non-transparent layer served as a mask by holding the X-ray radiation in order to produce a high-contrast (at least 20 : 1) signal. The masking layer thickness in the transparent mask is equal to tens nanometers, therefore the numerical experiment made an assumption for a non-transparent, infinitely thin mask with ideal holes.

Then the wavefront that has passed the object achieves the refractive lens. When the wavefront goes through the lens, a part of the diffracted radiation from the mask is lost due to the finite size of the geometrical lens aperture, while the other part is lost due to the radiation absorption in the lens material. It should be noted that in most cases the diffracted radiation loss from the mask (wavefront data) due

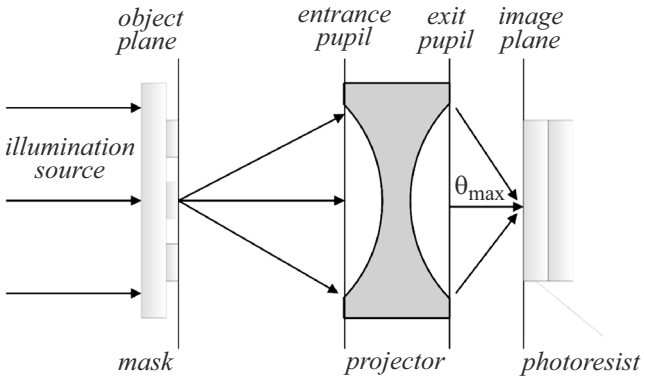

Figure 1. Diagram of image generation by the refractive X-ray optics on an X-ray nanolithography tool.

to absorption is much higher than due to the loss induced by the finite lens aperture. Ultimately, the „distorted“ wave front achieves the focal plane (X-ray resist wafer) with some reduction. The final image quality depends to a great extent on the amount of the wavefront data lost when the radiation goes through the lens.

CRL may be treated as a thin lens, therefore the following equation is valid for it:

$$\frac{1}{d}+\frac{1}{f}=\frac{1}{F}, \tag{1}$$

where F is the CRL focal distance, d is the distance from the object (transparent dynamic mask) to the lens, f is the distance from the lens to the image (the X-ray resist on the exposed wafer). The focal distance in turn can be calculated as follows

$$F = R/2\delta N, \tag{2}$$

where R is the curvature radius of the refractive lens surface, δ is the refraction index decrement $(n = 1 - \delta + i\beta)$, N is the number of elementary biconcave lens in CRL.

The main parameters of any optical system are the image reduction coefficient and numerical aperture NA that is defined by the aperture angle $\theta_{\max}$ and refraction index of medium between the lens and focal plane. Since the whole optical system is in vacuum, we will assume the refraction index equal to 1, therefore the following equation is valid for the numerical aperture

$$NA = \frac{A_{\text{eff}}}{2F}, \tag{3}$$

where A_{eff} is the effective geometrical aperture at the lens output. Geometrical lens aperture usually means the lens diameter. When the lens absorption is considered, then a Gaussian beam with a width lower than the geometrical aperture occurs. The Gaussian beam width is call in the literature as A_{eff} — the effective lens aperture.

The increased numerical aperture produces more detailed and high quality resist image. This is due to the fact that the refractive optics with higher NA collects more diffracted radiation from the object (transparent mask or pattern). Additional diffraction orders provide increasingly more distinct and contrast intensity distribution in the focal plane.

The optical system is characterized by optical transfer functions that may be obtained using various approaches. The most simple approach is to use idealized optical transfer functions, e.g. the Kirchhoff approach for an infinitely thin mask with ideal holes. There are more sophisticated and physical (qualitative) methods for optical transfer function calculation, e.g. rigorous calculation of electromagnetic radiation passing through the mask obtained using the mathematical simulation. It should be noted that the masking layer thickness in the transparent mask is equal to tens nanometers, therefore the numerical experiment made an assumption for a non-transparent, infinitely thin mask with ideal holes. However, depending on the transparent mask configuration and radiation wavelength, the masking layer is not always 100% non-transparent and a perfectly flat wave is not always observed at the output of the optical channel.

Suppose the radiation field at the set wavelength between the object plane and lens input plane is known in the object plane $z = 0$ and is defined by the vector fields $\mathbf{E}(x, y, 0)$, $\mathbf{H}(x, y, 0)$. The radiation field distribution in any point between the object plane and lens inlet plane may be found by solving the Helmholtz equation. The Helmholtz equation for any electric and magnetic field projection looks the same and, setting aside the polarization effects, the scalar theory may be sufficient. Then the Helmholtz equation will be written as

$$\Delta u + k^2 u = 0. \tag{4}$$

Here, the radiation field $u(x, y, z)$ is any electric or magnetic field projection. In our case, the X-ray radiation is in the form of a transverse wave, therefore, to be specific, assume that u is the electric field E_x projection.

Thus, find the solution of Helmholtz equation (4) with defined boundary condition $u(x, y, z = 0)$ on the object plane. To solve the problem, use the Fresnel–Kirchhoff integral:

$$u(\mathbf{r_0}) = -\frac{1}{4\pi}\iint\limits_{S_1} u(x, y, 0) 2ik \frac{e^{ikR}}{R}\left(1 - \frac{1}{ikR}\right)\frac{z_0}{R} dS. \tag{5}$$

Here, $R = \sqrt{(x - x_0)^2 + (y - y_0)^2 + z_0^2}$, S_1 is the object plane and integration is performed with respect to the (x, y) coordinates in the object plane. Point $P(x_0, y_0, z_0)$ is the point where the radiation field is sought for. Thus, z_0 is the distance from the object plane to the lens input plane and (x_0, y_0) are the observation point coordinates in the lens input plane.

It should be noted that the distance between the object plane (transparent mask) and lens input plane is by several orders of magnitude longer that the wavelength $(z_0 \gg \lambda)$, hence, $kR \gg 1$. In this approximation, integral (5) changes to the Fresnel–Kirchhoff integral:

$$u(\mathbf{r_0}) = -\frac{k}{4\pi i}\iint\limits_{S_1} u(x, y, 0)\frac{e^{ikR} z_0}{R^2} dS. \tag{6}$$

When considering an object whose typical size is much smaller than the distance between the object plane (transparent mask) and lens inlet plane, then in this case $|x|/z_0 \ll 1$ and $|y|/z_0 \ll 1)$ will be small parameters. Moreover, beams in this case will go at low angles to the Oz axis, i.e. they will be paraxial, therefore, $|x - x_0|/z_0 \ll 1$ and $|y - y_0|/z_0 \ll 1$ are also small parameters. This allows the distance R to be expanded into a Taylor series in small parameters $|x - x_0|/z_0$ and $|y - y_0|/z_0$, i.e. $R \approx z_0 + \left((x - x_0)^2 + (y - y_0)^2\right)/(2z_0)$. As a result of these approximations, integral (6) changes to the Fresnel

diffraction integral:

$$u(\mathbf{r_0}) = \frac{e^{ikz_0}}{i\lambda z_0} \int_{-\infty}^{\infty} dx \int_{-\infty}^{\infty} dy u_0(x,y) \times \exp\left[ik\frac{(x-x_0)+(y-y_0)}{2z_0}\right]. \quad (7)$$

2. Simulation of the composite kinoform lens parameters in the soft X-ray wavelength range

To understand how the refractive optics works, use an elementary biconcave lens shown in Figure 2.

The diffraction limit of resolution of the elementary refractive lens is calculated as follows

$$\Delta x = \frac{\lambda}{NA}. \quad (8)$$

By substituting equations (2) and (3) into equation (8), we get

$$\Delta x = \frac{\lambda R}{a\delta}, \quad (9)$$

where R is the refractive lens surface curvature radius, a is the lens radius equal to the half geometrical aperture of the lens.

CRLs are used in X-ray optics within the hard X-ray wavelength range ($\lambda < 1$ nm). This is facilitated by negligibly low X-ray absorption $\delta \sim 10^{-5}$–10^{-9} for these wavelengths. However, when changing to the soft X-ray wavelength, absorption in the lens material becomes more significant ($\delta \sim 10^{-2} \ldots 10^{-5}$ depending on the lens material and wavelength). Figure 3 shows the dependence of X-ray transmission by Si, Be and Diamond membrane on the X-ray wavelength and membrane thickness.

The figure shows that there is a material with transmission $T_{XR} > 10\%$ for 100 nm membranes for the whole wavelength range. But when the membrane thickness increases up to 1 μm, the transmission decreases dramatically and narrow wavelength ranges satisfy the condition: $\lambda < 3.6$ nm and $\lambda > 11.2$ nm for Be and $4.4 < \lambda < 6.8$ nm for diamond films. The foregoing suggests that strong X-ray absorption in the refractive lens material makes it difficult to use it as an element of an optical system in the selected wavelength range ($2 < \lambda < 14$ nm) at $p > 1000$ nm.

Thickness of the thinnest lens portion is usually $d \sim 0.1\,\mu$m, while the lens thickness will be equal to

$$p = d + \frac{a^2}{R}. \quad (10)$$

If $T_{XR} > 10\%$ is adhered to, then the maximum thickness of the Be lens is $p = 5.1\,\mu$m at $\lambda = 2$ nm. To estimate the numerical aperture NA of the Be lens depending on the lens surface curvature radius R, a graph is provided in Figure 4 showing that the numerical aperture NA increases as the curvature radius R decreases. However, a refractive lens with high numerical aperture $NA > 0.2$ may be obtained only at the surface curvature radii of $R \leq 10$ nm.

Thus, it can be said that it is difficult to select a refractive lens with high numerical aperture $NA > 0.2$ due to strong X-ray absorption in the lens material. A question arises: how we can reduce the lens loss? This problem may be solved by removing some lens material areas whose length is chosen in such a way as to ensure that the phase shift is a multiple of 2π [22,23]. The remaining part of the lens acts as a solid lens. Such lens is known as a diffraction lens. We describe the diffraction lens based on the lens shown in Figure 2. Remove some lens material by cutting horizontal stripes the length of which is a multiple of the

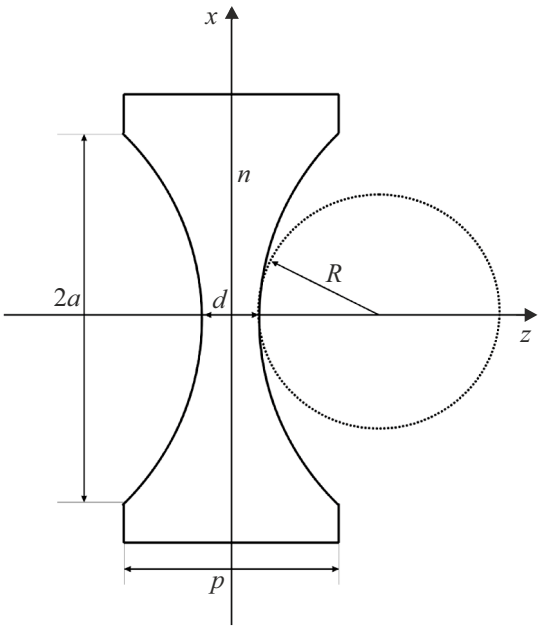

Figure 2. Elementary biconcave refractive X-ray lens; p is the lens thickness, R is the parabolic lens surface curvature radius, $2a$ is the lens diaphragm diameter, d is the lens neck thickness.

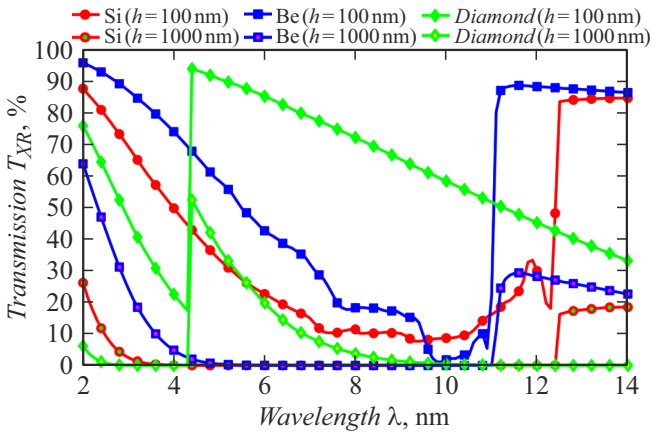

Figure 3. Dependence of X-ray transmission by the membrane (Si, Be, diamond) on the X-ray wavelength and membrane thickness.

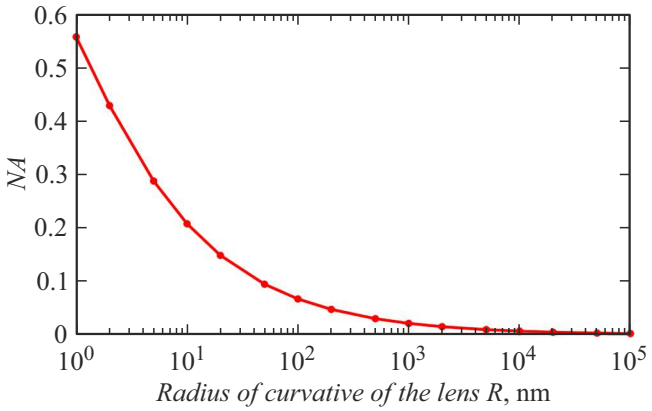

Figure 4. Dependence of the numerical aperture *NA* of the Be lens on the lens surface curvature radius R ($\lambda = 2$ nm).

phase shift 2π. Figure 5 shows a diagram of calculation of the diffraction lens components. On the top of the lens, there is a polygon that limits the removed lens material part in the form of n horizontal layers. Positions of points on the right parabola are calculated as $z_n = d/2 + nL_0$, $x_n = \sqrt{2RnL_0}$. The step length L_0 on the refractive surface is defined as follows $L_0 = M \cdot L_\pi$, $M = 2, 4, \ldots$, where $L_\pi = \lambda/2\delta$ is the length on which the phase shift is equal to π. Horizontal dimensions of the triangular steps are the same and the vertical dimensions are calculated as follows

$$\Delta x_n = x_{n+1} - x_n = \sqrt{2R \cdot L_0}(\sqrt{n+1} - \sqrt{n}). \qquad (11)$$

A kinoform type lens shall be also mentioned. Kinoform lenses fall in between the elementary refractive lenses and diffraction lenses. A kinoform lens may be obtained by shifting each diffraction lens step by $L = L_0 \cdot k$, where $k = 0, 1, 2 \ldots$ is the step number and $k = 0$ corresponds to the central step. Thus all step are in the same plane which is shown in Figure 6. The key structural parameters of the composite kinoform lens (CKL) are as follows: R — the radius of curvature of the refractive lens surface; L_0 — the kinoform lens step length; W_{center} — the central step length; W_{edge} — the edge step length; N — the number of elementary lenses in CKL; N_{step} — the number of steps in an elementary lens.

When selecting the lens material, consider δ — the refraction index decrement on this wavelength, because it defines the focal distance, numerical aperture and resolution of the lens. According to equation (2), the higher δ the lower the focal distance, therefore, the higher *NA* and lens resolution, respectively. Also consider the absorption coefficient β of the lens material for a particular wavelength that shall be as low as possible. Thus, a material with high δ and low β will be promising in terms of the refractive X-ray optics. Figure 7 shows the dependence of δ/β on the wavelength that is used to define promising materials for creation of kinoform (diffraction) lenses. In Figure 7, the best materials shall be distinguished in terms the highest δ/β on the particular wavelength intervals:

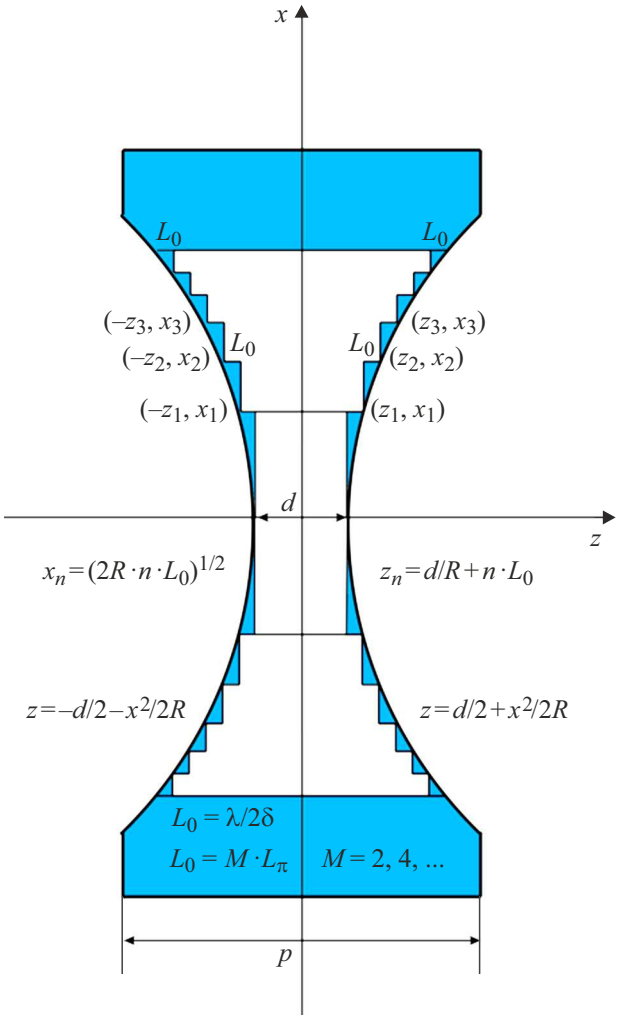

Figure 5. The diffraction lens obtained by removing some lens material areas whose length is chosen in such a way as to ensure that the phase progression is a multiple of 2π.

1) Be is the best material at $\lambda < 2.5$ nm;

2) BeO is the best material at $2.5 < \lambda < 4.5$ nm;

3) diamond is the best material at $4.5 < \lambda < 8$ nm;

4) diamond and B are the best materials at $8 < \lambda < 13.5$ nm;

5) Be is the best material at $\lambda > 14$ nm.

When the promising materials for various wavelengths had been defined, wavefront variation was simulated when passing different optical system areas:

1) from the transparent mask to the lens,

2) in the lens material considering the radiation absorption effect,

3) from the lens output plane to the focal plane (substrate plane with the X-ray resist).

For all calculations, a fourfold lens reduction was set, i.e. the photoresist pattern is assumed to be 4 times smaller than the size of holes in the transparent mask. The size of holes shall be selected such that to achieve the minimum

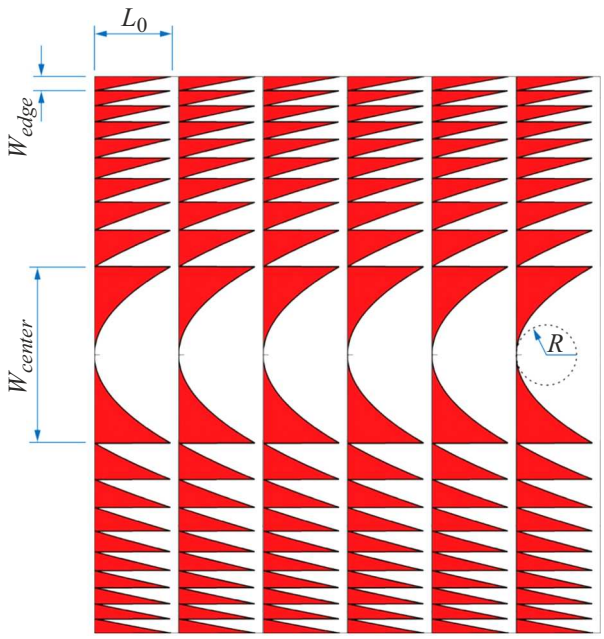

Figure 6. CKL. W_{center} — the central step length, W_{edge} — the edge step length, L_0 — the step length, R — the radius of curvatures of the refractive surface.

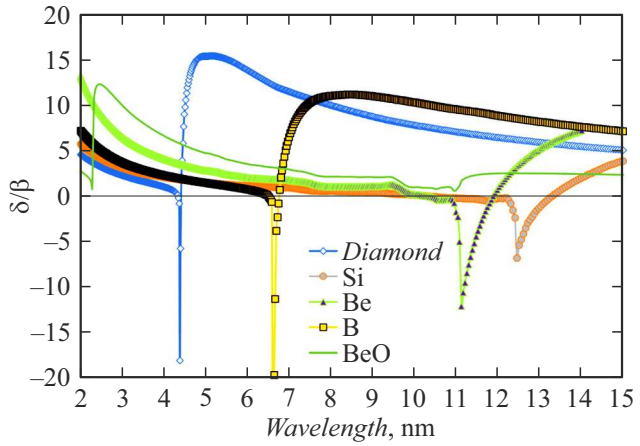

Figure 7. Dependence of δ/β (decrement δ of the refraction index vs. the absorption coefficient β) on the wavelength.

possible resolution (half pitch) for a particular wavelength and CKL material.

Radiation intensity in the focal plane of CKL was first calculated as shown in Figure 8 near 13.5 nm for Be, diamond and B. During the numerical simulation, the following parameters were chosen for the three materials: wavelength 13.5 nm, radius of curvature of the lens surface 1 μm. Numerical simulations demonstrated that diamond is the best material at $\lambda = 13.5$ nm and allows the half pitch of 28 nm to be achieved. Figure 8 shows that the diamond CKL has a sharp vertical profile of radiation intensity distribution and the minimum noise level (1.9%), that also supports the selection of diamond

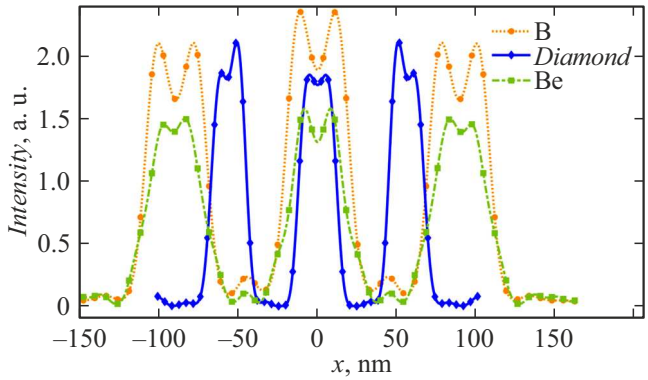

Figure 8. Radiation intensity distribution in the focal plane of CKL based on: Be, diamond, B. The image was obtained from the mask with three holes near 13.5 nm.

as the most promising material at 13.5 nm. It should be explained that the noise level is the ratio of the intensity of parasitic radiation falling into the CKL focal plane to the intensity of useful radiation in the CKL focal plane. Table 1 shows comparative parameters of CKL made of Be, diamond and B. For different materials and lens geometries, diffraction effects occur at step edges, taking into account decrements δ of the refraction index, this introduces a limit to the lens resolution increase. Table 1−5 lists the CKL parameters for which the best results for the CKL resolution have been obtained.

Radiation near $\lambda = 8$ nm was also analyzed. According to Figure 7, diamond and B are the most promising materials at this wavelength. Therefore, mathematical simulation was carried out to obtain the intensity distribution in the focal plane as shown in Figure 9 from the transparent mask with three holes. Like in the first case ($\lambda = 13.5$ nm), numerical simulation for the three materials recorded the following parameters: wavelength 8 nm, radius of curvature of the lens surface 1 μm. CKL made of diamond and B have shown the same half pitch — 28 nm. The diamond CKL

Table 1. Parameters of CKL based on various materials Be, diamond, B for radiation $\lambda = 13.5$ nm

Parameter	Lens material		
	Be	Diamond	B
Half pitch resolution, nm	45	28	45
Number of lenses	4	2	4
Noise level, %	7.2	1.9	11.1
Radiation intensity, a.u.	1.5	1.85	2
Energy loss in CKL, %	62.5	53.75	50
numerical aperture NA	0.693	0.774	0.605
Focal distance F, μm	26.03	20.44	7.903
Theoretical lens resolution, nm	19.5	17.4	22.3
Number of lens steps	888	2264	168
Lens step length, nm	703	110	213
Central step width, nm	1186	743	653
Edge step width, nm	28	11	36

Table 2. Parameters of CKL based on various materials (diamond, B) for radiation wavelength $\lambda = 8$ nm

Parameter	Lens material	
	Diamond	B
Half pitch resolution, nm	28	28
Number of lenses	4	6
Radiation intensity, a.u.	2.05	1.76
Energy loss in CKL, %	48.75	56
Noise level, %	4.9	7.4
Numerical aperture *NA*	0.637	0.605
Focal distance F, μm	12.11	20.21
Theoretical lens resolution, nm	12.6	11.4
Number of lens steps	516	824
Lens step length, nm	194	485
Central step width, nm	623	985
Edge step width, nm	19.4	24.2

Table 3. Parameters of CKL based on various materials (diamond, BeO) for radiation wavelength $\lambda = 5$ nm

Parameter	Lens material	
	Diamond	BeO
Half pitch resolution, nm	20	28
Number of lenses	8	4
Radiation intensity, a.u.	1.35	1
Energy loss in CKL, %	66.25	75
Noise level, %	2.6	11.4
Numerical aperture *NA*	0.502	0.398
Focal distance F, μm	103.4	28.85
Theoretical lens resolution, nm	10	12.6
Number of lens steps	1740	540
Lens step length, nm	414	289
Central step width, nm	2034	760
Edge step width, nm	34.5	23.1

Table 4. Parameters of CKL based on various materials (BeO, Be) for radiation wavelength $\lambda = 3$ nm

Parameter	Lens material	
	Be	BeO
Half pitch resolution, nm	20	20
Number of lenses	6	6
Radiation intensity, a.u.	0.8	1.3
Energy loss in CKL, %	80	67.5
Noise level, %	6.6	5.5
Numerical aperture *NA*	0.309	0.335
Focal distance F, μm	77.1	56.27
Theoretical lens resolution, nm	9.7	9
Number of lens steps	900	788
Lens step length, nm	694	506
Central step width, nm	1178	1006
Edge step width, nm	27.8	25.3

Table 5. Parameters of CKL based on various materials (Be, B, Si, diamond) for radiation wavelength $\lambda = 2$ nm

Parameter	Lens material			
	Be	B	Si	Diamond
Half pitch resolution, nm	14	14	14	14
Number of lenses	14	10	10	6
Radiation intensity, a.u.	0.8	0.5	0.38	0.48
Energy loss in CKL, %	80	87.5	90.5	88
Noise level, %	12.5	14	15.3	8.6
Numerical aperture *NA*	0.467	0.448	0.433	0.428
Focal distance F, μm	75.85	79.94	83.33	84.47
Theoretical lens resolution, nm	4.3	4.5	4.6	4.7
Number of lens steps	1506	2000	1920	3156
Lens step length, nm	1062	800	833	507
Central step width, nm	1457	1264	1291	1007
Edge step width, nm	26.5	20	20.8	12.7

contained 4 elementary lenses in contrast to the boron lens that contained 6 elementary lenses, therefore the intensity of the former is 16% higher and the noise level is 3.5% lower. Thus, it is suggested that the diamond CKL at $\lambda = 8$ nm is the best material for achievement of the best lithography results. Table 2 shows comparative parameters of diamond and B CKLs.

The next investigation stage was to determine the most promising material at $\lambda = 5$ nm. Data in Figure 7 show that diamond hold a lead in δ/β at this wavelength. Therefore diamond has been selected as a lens material for optical system calculations. Besides diamond, we analyzed BeO that also has high δ/β at $\lambda = 5$ nm. Figure 10 shows numerical simulation results that provided radiation intensity distribution ($\lambda = 5$ nm) in the focal plane obtained from the transparent mask with three holes for the optical system with diamond and BeO CKLs. The following parameters were selected during the simulation: wavelength $\lambda = 5$ nm, radius of curvature of the lens surface $R = 1\,\mu$m, image reduction — 4-fold. The numerical simulation results supported the data in Figure 7: using the diamond CKL, a half pitch of 20 nm may be achieved. It should be also noted that the radiation intensity in the focal plane of the diamond lens is higher by 35% than that of the BeO lens and the noise level is lower by 8.8%. Further, Table 3 is given to compare the diamond and beryllium oxide CKL parameters.

The next investigated area of the soft X-ray range was in the vicinity of $\lambda = 3$ nm. Figure 7 shows that Be and BeO are the most promising materials in this area. Therefore, numerical calculation of radiation distribution in the Be and BeO CKL optical system was performed and gave radiation intensity distribution in the focal plane from the transparent mask with three holes. The radiation intensity distribution is shown in Figure 11. Like in the previous cases, the following parameters were chosen during the

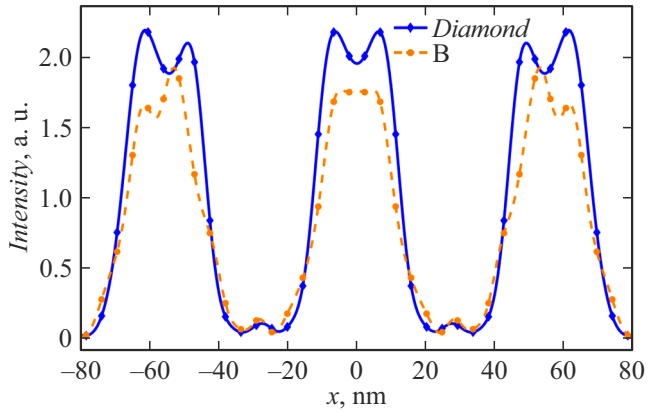

Figure 9. Radiation intensity distribution in the focal plane of CKL based on: diamond, B. The image was obtained from the mask with three holes near 8 nm.

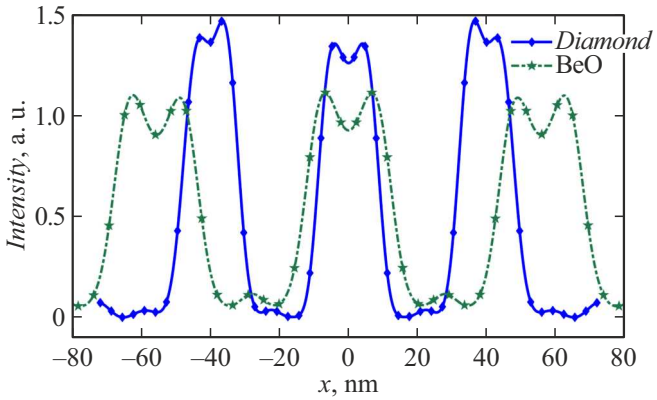

Figure 10. Radiation intensity distribution in the focal plane of CKL based on: diamond, BeO. The image was obtained from the mask with three holes near 5 nm.

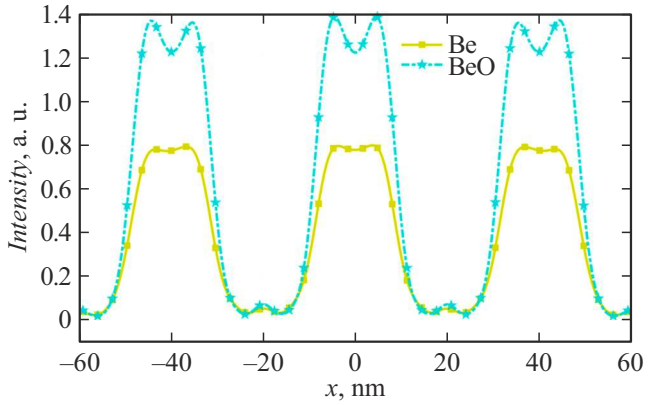

Figure 11. Radiation intensity distribution in the focal plane of CKL based on: Be, BeO. The image was obtained from the mask with three holes near 3 nm.

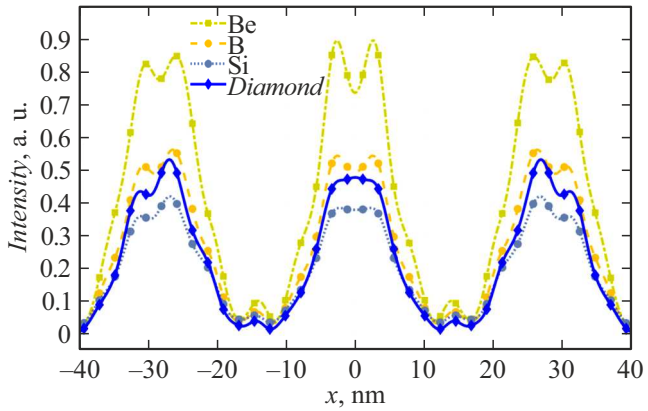

Figure 12. Radiation intensity distribution in the focal plane of CKL based on: Be, B, Si and diamond. The image was obtained from the mask with three holes near 2 nm.

simulation: wavelength $\lambda = 3$ nm, radius of curvature of the lens surface $R = 1\,\mu$m, image reduction — 4-fold. From Figure 11 it is easy to see that Be and BeO lenses may be used to achieve a resolution of 20 nm, but the radiation intensity in the focal plane obtained using BeO CKL is higher by 60%. Table 4 shows comparative optical system parameters of the Be and BeO CKLs.

X-ray radiation near $\lambda = 2$ nm is also of great interest. Figure 7 shows that as many as several materials are promising at this wavelength: Be, B, Si and diamond. Numerical simulation of the optical system of CKLs made of the abovementioned materials was performed to obtain intensity distribution in the focal plane as shown in Figure 12. The following parameters were selected during the calculations: wavelength $\lambda = 2$ nm, radius of curvature of the lens surface $R = 1\,\mu$m, image reduction — 4-fold. The numerical simulation results show that all abovementioned materials are used to produce CKLs with a half pitch resolution of 14 nm at this wavelength ($\lambda = 2$ nm). Figure 12 shows that the highest intensity may be achieved using the Be CKL composed of 14 elementary lenses. It should be also noted that the lowest noise level may be achieved using the diamond CKL system consisting of 6 elementary lenses. The comparative parameters of CKL are shown in Table 5.

To sum up the interim results, it can be said that wavelength reduction is used to achieve a higher half pitch; and the radiation intensity decreases due to using more elementary lenses in CKL. Among the parameters characterizing the optical system, the following key parameters may be distinguished: half pitch of the optical system, relative intensity, noise level.

According to these criteria, based on the simulation results, the most successful materials and wavelength intervals shall be defined. Diamond kinoform lens are leading at a large wavelength segment: $4.4 < \lambda < 14$ nm. This interval is limited on the left side by the sign change of δ of the refraction index at $\lambda \sim 4.3$ nm (Figure 7). It should be also noted that diamond has outstanding thermal conductivity (900–2300 W/(m·K)) that facilitates fast heat removal from the optical system. Then, $2.4 < \lambda < 4.4$ nm interval follows where BeO is more preferable. This interval

is limited on the left side with reduction of decrement δ of the refraction index for BeO at $\lambda \sim 2.3$ nm due to the oxygen atom content whose decrement δ of the refraction index changes sign near $\lambda \sim 2.3$ nm. In the extreme left $\lambda < 2.3$ nm interval, Be is preferred because it has the highest δ/β, and the maximum radiation intensity in the focal plane was obtained using the Be lenses.

By means of an example of the optical system of Be kinoform lens, the effect of the lens entrance pupil aperture and, accordingly, of the numerical aperture NA on the signal waveform (wavefront) in the focal plane was analyzed. The following system parameters were taken during the numerical calculations: X-ray wavelength $\lambda = 2$ nm, number of elementary lenses — 6, number of holes in the transparent mask — 7, fourfold reduction of the optical system.

Figure 13 shows the dependence of the wavefront form in the focal plane on the entrance pupil aperture radius a. In the first case (Figure 13, a), the aperture radius is $a = 30\,\mu$m ($NA = 0.067$). In this case, the intensity distribution is uniform without any pronounced peaks. This is explained by the act that insufficient amount of diffracted radiation enters the lens entrance pupil which is confirmed by the wavefront amplitude graph that shown only the central diffraction order.

Figure 13, b shows the wavefront intensity distribution in the focal plane for the entrance pupil aperture radius $\alpha = 45\,\mu$m ($NA = 0.101$). This figure shows pronounced peaks in the intensity distribution and their number corresponds to the number of holes in the transparent mask. This qualitative improvement of the intensity distribution is explained by appearance of an additional diffraction order in the wave front at the input and output of the optical system. However, the peak intensity is nonuniform — central peaks have higher intensity than the edge peaks.

Then, Figure 13, c shows the doubled aperture radius $a = 90\,\mu$m ($NA = 0.197$). Peak intensity in the focal plane has become more uniform — the edge peaks have almost the same intensity as the central ones. However, like in Figure 13, b, the intensity of each separate peak has a normal distribution form (Gaussian distribution) that is insufficient for lithography because the initial process pattern will be distorted on the exposed wafer due to a small number of diffraction orders falling on the lens entrance pupil.

In Figure 13, d, the lens entrance pupil aperture radius is $a = 125\,\mu$m ($NA = 0.27$). The wavefront amplitude graph shows that the second diffraction order falls on the lens entrance pupil allowing to get additional wavefront data. On the graph of the radiation intensity in the focal plane, intensity of a separate peak has not got the Gaussian distribution form any more because the intensity of each peak achieves the „shelf“. Thus, it can be said that the minimum number of diffraction orders necessary for proper image transfer to an X-ray resist is equal to 2.

Dependence of the effect of the number N of elementary lenses in CKL on the wavefront quality in the focal plane was investigated. For this, the optical system consisting of beryllium kinoform lens was analyzed at $\lambda = 2$ nm. Beryllium at this wavelength is the most suitable for demonstration of this dependence because it has minimum absorption allowing a large number of lenses to be used. The lens entrance pupil aperture radius was equal to $R = 5\,\mu$m, image reduction was — 4-fold.

Figure 14 shows the numerical calculation of Be CKLs for with varying number N of elementary lenses. In Figure 14, a, CKL consisted of $N = 2$ elementary lenses. The numerical aperture of such system $NA = 0.076$, which is insufficient to produce a good X-ray resist image because the intensity distributions of each separate peak have a normal distribution form. This is associated with the fact

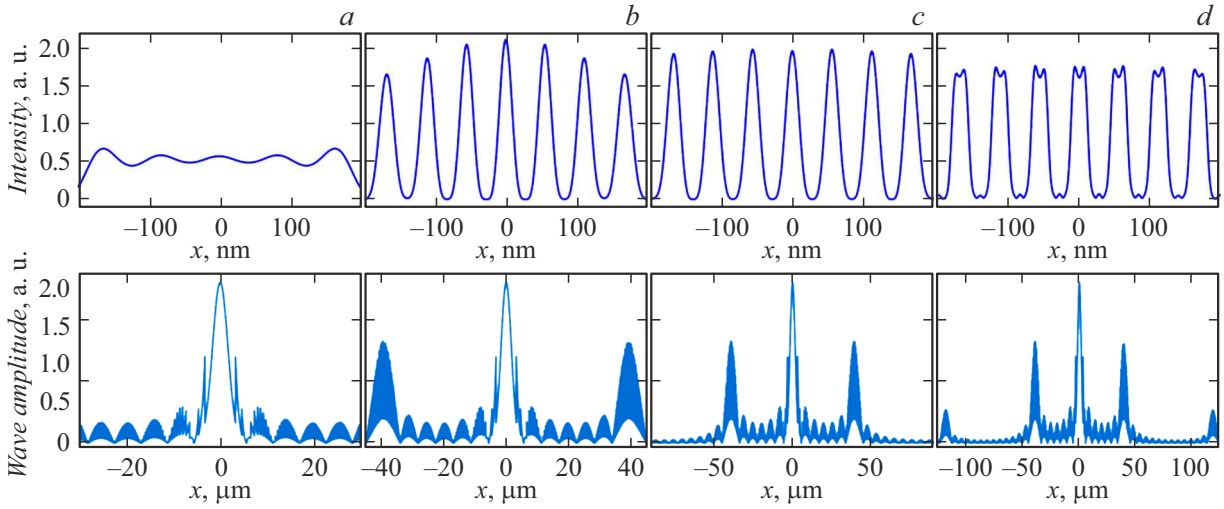

Figure 13. Dependence of radiation intensity distribution in the focal plane and wavefront distribution at the CKL outlet from various lens entrance pupil aperture radii:a — $a = 30\,\mu$m ($NA = 0.067$); b — $a = 45\,\mu$m ($NA = 0.101$); c — $a = 90\,\mu$m ($NA = 0.197$); d — $a = 125\,\mu$m ($NA = 0.27$).

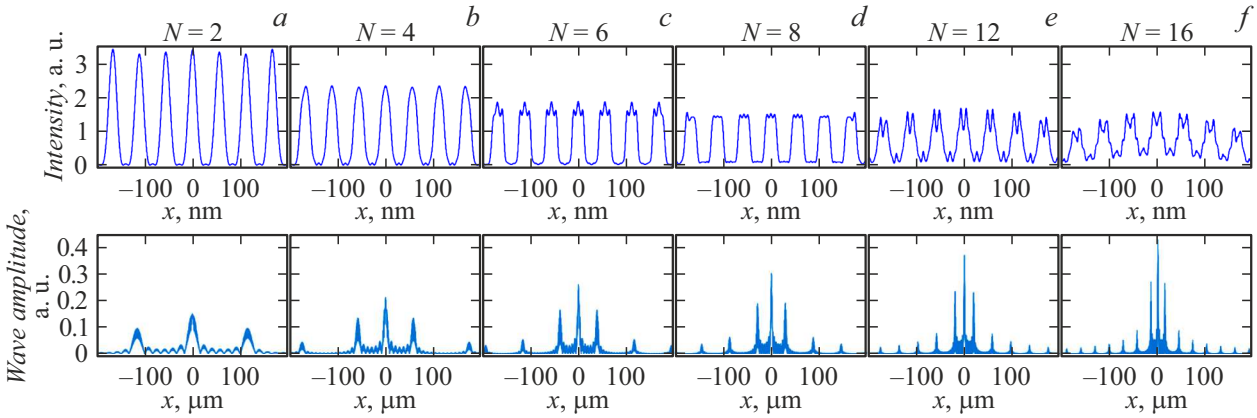

Figure 14. Distribution of radiation intensity in the focal plane and of wavefront at the CKL outlet depending on the number of elementary lenses: *a* — $N = 2$ ($NA = 0.076$); *b* — $N = 4$ ($NA = 0.151$); *c* — $N = 6$ ($NA = 0.223$); *d* — $N = 8$ ($NA = 0.292$); *e* — $N = 12$ ($NA = 0.416$); *f* — $N = 16$ ($NA = 0.521$).

that only the central and first diffraction order falls into the lens entrance pupil aperture.

Then, in Figure 14, *b*, the number of the elementary lenses is doubled, thus, the numerical aperture is almost doubled $NA = 0.151$. The Figure shows that the entrance pupil has one additional diffraction order, however, the intensity distributions still have a normal distribution form, but the distribution form becomes increasingly closer to a square-wave signal that produces a good diffraction pattern.

CKL in Figure 14, *c* consists of 6 elementary lenses, whereas the numerical aperture $NA = 0.223$. The additional diffraction order made it possible to obtain a nearly square-wave intensity distribution in the focal plane. As for Figure 14, *a*–*c*, it should be noted that the intensity decreases proportionally to the number N of elementary lenses.

In Figure 14, *d*, the number of elementary lenses is increased up to 8 and the numerical aperture is increased up to $NA = 0.292$. The figure shows that the intensity distribution is close to the square-wave distribution allowing a high-quality X-ray resist pattern to be produced.

Figure 14, *e*,*f* shows that further increase in the number of elementary lenses in CKL results in sharp rise of the noise level in the central intensity distribution region in the focal plane and, consequently, to the difference in intensity levels in the center and on edges.

Thus, it is necessary to conclude that the increase in the number of elementary lenses in CKL results in the increase of the numerical aperture which in turn improves the intensity distribution quality in the focal plane. However, this also results in the decrease of intensity and increase of the noise interference level. Therefore the optimum number of elementary lenses in CKL shall be chosen individually depending on both the radiation wavelength and lens material.

3. Evaluation of the performance of a X-ray lithograph based on a kinoform lens system

The flat wavefront with a diameter of 10 mm from the SS source falls on the illuminating optical system that compresses the beam in one direction to 10 μm. Then, the compressed beam illuminates the transparent mask (Figure 1). The SS beam power P_S depending on the wavelength varies from 3 to 20 W. CKL downstream of the transparent mask focuses the X-ray radiation onto the X-ray resist wafer having a sensitivity of $D = 20\,\text{mJ/cm}^2$. Considering the energy loss (50%) in the optical system that compresses the synchrotron beam before it enters the transparent mask, we obtain the radiation power density on the transparent mask: $P_{TM} = 0.5P_S/S$, where S is the transparent mask area. Knowing the energy loss p_{los} and reduction ratio $k = 4$ in CKL, the X-ray resist power density may be estimated: $P_R = P_{TM}(1 - p_{los})k^2$. Pixel patterning time on the X-ray resist is calculated as follows $\tau_{pix} = D/P_R$. If median values $P_S = 10$ W and $p_{los} = 0.6$ are taken, then the single pixel patterning time on the X-ray resist will be $\tau_{pix} = 0.65\,\mu$s.

The wafer patterning rate using the X-ray lithograph based on the CKL system is limited, on the one hand, by the dimensions of the lens entrance pupil (about 1 mm) and the exposed area of the transparent mask and,on the other hand, by the response time $\tau_{MEMS} = 20\,\mu$s of the MEMS gate that opens or closes the required optical channel. The total time of one patterning cycle is $\tau = \tau_{MEMS} + \tau_{pix} = 20.65\,\mu$s. The transparent mask has a set of holes arranged in line with a ratio of the hole size to the period between the holes equal to 1 : 3. Taking into account the fourfold reduction of the CKL optical system, the 112 nm square holes shall be used to obtain a 28×28 nm pixel. Thus, the number of holes in the transparent mask fitting the 1 mm segment is equal to $N \approx 3 \cdot 10^3$. Hence, for a single 28×28 nm pixel, we get an area exposed during one cycle of about $S_{cycle} = 2.35\,\mu\text{m}^2$.

Since the effective area of 200 mm wafer $S_{\text{eff}} = 2 \cdot 10^4\,\text{mm}^2$, the number of cycles $M = S_{\text{eff}}/S_{cycle} = 8.5 \cdot 10^9$, and the exposure time is $t_{\text{tot}} = \tau M \approx 48\,\text{h}$.

Conclusion

The study shows that composite refractive optical systems may be produced on the basis of kinoform lenses in the soft X-ray wavelength range ($\lambda = 2-14\,\text{nm}$). The simulation has shown that the transfer from standard refractive lenses to kinoform lenses reduces absorption considerably allowing the lens resolution to be increased. The numerical simulation defined the best materials for the whole soft X-ray wavelength range. Diamond kinoform lenses are most preferable on a large wavelength interval $4.4 < \lambda < 14\,\text{nm}$. In the wavelength interval $2.4 < \lambda < 4.4\,\text{nm}$, BeO is the most promising material for the refractive optics. Beryllium (Be) kinoform lenses ensure the best result in the wavelength region $\lambda < 2.4\,\text{nm}$. It has been established that as the wavelength decreases, a larger number of elementary lenses may be used in CKL because a decreasing tendency of absorption coefficient β and decrement δ is seen for most materials with decreasing wavelength. The simulation has shown that the maximum half pitch that can be achieved using CKL in the soft X-ray range is 14 nm at $\lambda = 2\,\text{nm}$ for Be, diamond, BeO and Si.

The numerical calculations gave the dependence of radiation intensity in the focal plane (exposed X-ray resist wafer plane) on the entrance pupil aperture radius. Dependence of the radiation intensity in the focal plane on the number of elementary lenses in CKL has been also analyzed. It is necessary to conclude that the increase in the number of elementary lenses in CKL results in the increase of the numerical aperture which in turn improves the intensity distribution quality in the focal plane. However, this also results in the decrease of intensity and increase of the noise interference level. Therefore the optimum number of elementary lenses in CKL for each particular configuration shall be chosen individually depending on both the radiation wavelength and lens material. The study results may be used in the development of a lithography system based on the transparent mask and CKL.

Funding

The study was supported by the Ministry of Science and Higher Education of the Russian Federation (State Assignment No. FSMR-2024-0003)

Conflict of interest

The authors declare that they have no conflict of interest.

References

[1] D.V. Sirotin. Econ. Rev. Rus., **3** (69), 105 (2021). DOI: 10.37930/1990-9780-2021-3-69-105-122

[2] N.N. Kulikova. Teoriya i praktika obshchestvennogo razvitiya, **12**, 87 (2017). DOI: 10.24158/tipor.2017.12.19

[3] V. Bakshi. *EUV Lithography*, Second edition (SPIE Press, Bellingham, Washington, USA, 2018)

[4] C. Smeets, N. Benders, F. Bornebroek, J. Carbone, R. Van Es, A. Minnaert, G. Salmaso, S. Young. *Optical and EUV Nanolithography XXXVI*, ed. by A. Lio, M. Burkhardt (SPIE, San Jose, United States, 2023), p. 9, DOI: 10.1117/12.2658046

[5] S. Amano, K. Masuda, A. Shimoura, S. Miyamoto, T. Mochizuki. Appl. Phys. B, **101** (1–2), 213 (2010). DOI: 10.1007/s00340-010-3997-7

[6] M. Richardson, C.-S. Koay, K. Takenoshita, C. Keyser, M. Al-Rabban. J. Vacuum Sci. Technol. B: Microelectronics and Nanometer Structures Processing, Measurement, and Phenomena, **22** (2), 785 (2004). DOI: 10.1116/1.1667511

[7] N.I. Chkhalo, K.V. Durov, A.N. Nechay, A.A. Perekalov, V.N. Polkovnikov, N.N. Salashchenko. J. Surf. Investig., **17** (S1), S226 (2023). DOI: 10.1134/S1027451023070078

[8] V.N. Polkovnikov, N.N. Salashchenko, M.V. Svechnikov, N.I. Chkhalo. Phys.-Usp., **63** (1), 83 (2020). DOI: 10.3367/UFNe.2019.05.038623

[9] N.I. Chkhalo, S.A. Gusev, A.N. Nechay, D.E. Pariev, V.N. Polkovnikov, N.N. Salashchenko, F. Schäfers, M.G. Sertsu, A. Sokolov, M.V. Svechnikov, D.A. Tatarsky. Opt. Lett., **42** (24), 5070 (2017). DOI: 10.1364/OL.42.005070

[10] N.I. Chkhalo, N.N. Salashchenko. AIP Adv., **3** (8), 082130 (2013). DOI: 10.1063/1.4820354

[11] C. Montcalm, S. Bajt, P. Mirkarimi, E. Spiller, F. Weber, J. Folta. SPIE, **3331**, 42 (1998). DOI: 10.1117/12.309600

[12] M.V. Svechnikov, N.I. Chkhalo, S.A. Gusev, A.N. Nechay, D.E. Pariev, A.E. Pestov, V.N. Polkovnikov, D.A. Tatarskiy, N.N. Salashchenko, Y.A. Vainer, M.V. Zorina, F. Schafers, M.G. Sertsu, A. Sokolov. Opt. Express, **26** (26), 33718 (2018). DOI: 10.1364/OE.26.033718

[13] D.S. Kuznetsov, A.E. Yakshin, J.M. Sturm, R.W.E. Van De Kruijs, E. Louis, F. Bijkerk. Opt. Lett., **40** (16), 3778 (2015). DOI: 10.1364/OL.40.003778

[14] C. Burcklen, S. de Rossi, E. Meltchakov, D. Dennetiere, B. Capitanio, F. Polack, F. Delmotte. Opt. Lett., **42** (10), 1927 (2017). DOI: 10.1364/OL.42.001927

[15] I.A. Artyukov, Y. Bugayev, O.Yu. Devizenko, R.M. Feschenko, Y.S. Kasyanov, V.V. Kondratenko, S.A. Romanova, S.V. Saveliev, F. Schafers, T. Feigl, Y.A. Uspenski, A.V. Vinogradov. Proc. SPIE, **5919**, 59190E (2005). DOI: 10.1117/12.620037

[16] I. Snigireva, M. Polikarpov, A. Snigirev. Synchrotron Radiation News, **34** (6), 12 (2021). DOI: 10.1080/08940886.2021.2022387

[17] V.G. Kohn, JETP Lett., **76** (10), 600 (2002). DOI: 10.1134/1.1541043

[18] V. Kohn, I. Snigireva, A. Snigirev. Opt. Commun., **216** (4–6), 247 (2003). DOI: 10.1016/S0030-4018(02)02285-X

[19] A. Snigirev, V. Kohn, I. Snigireva, B. Lengeler. Nature, **384** (6604), 49 (1996). DOI: 10.1038/384049a0

[20] A. Snigirev, V. Kohn, I. Snigireva, A. Souvorov, B. Lengeler. Appl. Opt., **37** (4), 653 (1998). DOI: 10.1364/AO.37.000653

[21] V.G. Kohn, M.S. Folomeshkin. J. Synchrotron Rad., **28** (2), 419 (2021). DOI: 10.1107/S1600577520016495

[22] V. Aristov, M. Grigoriev, S. Kuznetsov, L. Shabelnikov, V. Yunkin, T. Weitkamp, C. Rau, I. Snigireva, A. Snigirev, M. Hoffmann, E. Voges. Appl. Phys. Lett., **77** (24), 4058 (2000). DOI: 10.1063/1.1332401

[23] D. Faklis, G.M. Morris. Appl. Opt., **34** (14), 2462 (1995). DOI: 10.1364/AO.34.002462

Translated by E.Ilinskaya

Translated by E.Ilinskaya